Intermittent hypoxia mediated by TSP1 dependent on STAT3 induces cardiac fibroblast activation and cardiac fibrosis

Qiankun Bao[1]*, Bangying Zhang[1], Ya Suo[1], Chen Liu[2], Qian Yang[1], Kai Zhang[1], Ming Yuan[1], Meng Yuan[1], Yue Zhang[1], Guangping Li[1]*

[1]Tianjin key laboratory of Ionic-Molecular Function of Cardiovascular Disease, Department of Cardiology, Tianjin Institute of Cardiology, The Second Hospital of Tianjin Medical University, Tianjin, China; [2]Department of Clinical Laboratory, Peking University People's Hospital, Beijing, China

Abstract Intermittent hypoxia (IH) is the predominant pathophysiological disturbance in obstructive sleep apnea (OSA), known to be independently associated with cardiovascular diseases. However, the effect of IH on cardiac fibrosis and molecular events involved in this process are unclear. Here, we tested IH in angiotensin II (Ang II)-induced cardiac fibrosis and signaling linked to fibroblast activation. IH triggered cardiac fibrosis and aggravated Ang II-induced cardiac dysfunction in mice. Plasma thrombospondin-1 (TSP1) content was upregulated in both IH-exposed mice and OSA patients. Moreover, both in vivo and in vitro results showed IH-induced cardiac fibroblast activation and increased TSP1 expression in cardiac fibroblasts. Mechanistically, phosphorylation of STAT3 at Tyr705 mediated the IH-induced TSP1 expression and fibroblast activation. Finally, STAT3 inhibitor S3I-201 or AAV9 carrying a periostin promoter driving the expression of shRNA targeting Stat3 significantly attenuated the synergistic effects of IH and Ang II on cardiac fibrosis in mice. This work suggests a potential therapeutic strategy for OSA-related fibrotic heart disease.

*For correspondence:
baoqiankun@tmu.edu.cn (QB);
tic_tjcardiol@126.com (GL)

Competing interests: The authors declare that no competing interests exist.

Introduction

The prevalence of sleep apnea is high in patients with cardiovascular disease, which could be caused by multiple risk factors including respiratory instability, obesity and upper airway dysfunction (*Javaheri et al., 2017*; *Kasai et al., 2012*). Sleep apnea, classified as obstructive sleep apnea (OSA) and central sleep apnea, affects or covaries with numerous health outcomes and physiological processes, particularly cardiovascular disease (*Javaheri et al., 2017*; *Kasai et al., 2012*; *Somers et al., 2008*). A recent prospective study of OSA found it associated with increased risk of incident heart failure in community-dwelling middle-aged and older men (*Gottlieb et al., 2010*). OSA is associated with a profile of perturbations that include sympathetic nerve activity, metabolic dysregulation, inflammation, oxidative stress, vascular endothelial dysfunction, and intermittent hypoxia (IH), all of which are critical for the pathogenesis of coronary heart disease, hypertension, atrial fibrillation, and heart failure (*Javaheri et al., 2017*; *Kasai et al., 2012*). IH is a hallmark of OSA and initiates several mechanisms that lead to cardiac fibrosis and cardiac dysfunction (*Baguet et al., 2012*; *Wei et al., 2016*).

Cardiac fibrosis is characterized by excessive deposition of extracellular matrix proteins by cardiac fibroblasts (CFs), which respond to pathological stress and environmental stimuli by transforming into myofibroblasts. Activated CFs express elevated levels of various proinflammatory and profibrotic factors causing fibroblast proliferation, migration and scar formation (*Travers et al., 2016*). The persistence of myofibroblasts eventually results in adverse changes in ventricular structure and

compliance, thereby leading to heart failure (*Baguet et al., 2012*; *Travers et al., 2016*). However, the effect and mechanism of CF activation in IH-induced cardiac remodeling remain unclear.

One central cytokine linked to cardiac fibrosis is transforming growth factor β (TGFβ), which is highly regulated at the level of activation (*Travers et al., 2016*; *Meng et al., 2016*). The activation of latent pro-TGFβ requires thrombospondin-1 (TSP1, encoded by *Thbs1* gene), which is a matricellular glycoprotein and can be secreted by various cell types, to remove its latency-associated propeptide (*Meng et al., 2016*; *Crawford et al., 1998*; *Adams and Lawler, 2011*). Myocardial TSP1 expression was increased in a mouse model of pressure overload because of transverse aortic constriction (*Xia et al., 2011*), and blocking TSP1-dependent TGFβ activation prevented cardiac fibrosis progression and improved cardiac function (*Belmadani et al., 2007*). However, the role and underlying mechanism of TSP1 in IH-induced CF activation and cardiac fibrosis remain to be elucidated.

As a member of the signal transducer and activator of transcription (STAT) protein family, STAT3 was originally identified as an interleukin-6–activated transcription factor. It can also be phosphorylated by receptor-associated Janus kinase (JAK) in response to growth factor and hemodynamic stress, thus acting as a regulator in fundamental cellular processes including inflammation, cell growth, proliferation, differentiation, migration, and apoptosis (*Wei et al., 2003*; *Chakraborty et al., 2017*; *He et al., 2018*). Emerging evidence demonstrates that STAT3 signaling is hyperactivated in fibrotic diseases, which may be an important molecular checkpoint for tissue fibrosis (*Chakraborty et al., 2017*; *Su et al., 2017*). Recent study demonstrated that STAT3 can drive TSP1 expression in astrocytes (*Tyzack et al., 2014*). Given the integrated function of STAT3 activation in inflammation and fibrosis, we hypothesized that IH-induced STAT3 activation might play a crucial role in CF activation and cardiac fibrosis by increasing TSP1 expression.

In the present study, we investigated the effect of IH exposure on cardiac fibrosis in response to angiotensin II (Ang II) in mice and the potential underlying mechanism. TSP1 expression induced by IH in CFs, mediated by phosphorylation of STAT3 at Tyr705, was involved in CF activation and cardiac fibrosis. Pharmacological or genetic inhibition of STAT3 restrained IH-induced CF activation and cardiac fibrosis and ameliorated IH-induced cardiac dysfunction.

Results

IH induced cardiac fibrosis and aggravated Ang II-induced cardiac dysfunction in mice

Most respiratory events of patients with OSA result in desaturation–reoxygenation sequences that cause IH (*Baguet et al., 2012*). To investigate IH exposure to cardiac function, we housed mice under IH or normoxia for 28 days (*Figure 1A*). Hypoxia in heart tissue was evaluated by using pimonidazole (*Figure 1—figure supplement 1A*). IH exposure slightly increased the ratio of heart weight to tibial length (*Figure 1B*). Echocardiography analysis revealed a moderate decrease in ejection fraction (EF) and fractional shortening (FS) with IH as compared with normoxia (*Figure 1C–D*). Furthermore, Masson and Sirius red staining demonstrated mildly larger fibrosis area in the heart of mice after IH exposure (*Figure 1E–F*).

To investigate the effect of IH associated with cardiac function after injury, we used the mouse model of Ang II-induced cardiac hypertrophy to represent cardiac fibrotic responses. Consistent with previous studies (*Su et al., 2017*; *Schafer et al., 2017*), Ang II treatment induced cardiac fibrosis with increasing the ratio of heart weight to tibial length and fibrosis area and impaired EF and FS (*Figure 1B–D*). Strikingly, IH exposure further impaired cardiac function, with increasing the ratio of heart weight to tibial length and decreasing EF and FS (*Figure 1B–D*). IH exposure significantly enlarged the fibrotic area of heart as well (*Figure 1E–F*). IH exposure had little effect on myocyte size or ratio of apoptotic cells in the left ventricle with or without Ang II challenge (*Figure 1—figure supplement 1B–C*). These results indicated that IH could induce cardiac fibrosis both at the basal level and in response to Ang II and also aggravated Ang II-induced cardiac dysfunction.

IH induced fibroblast activation in myocardial interstitium

CFs are now recognized for their fundamental contributions to the heart's response to various forms of injury (*Travers et al., 2016*). To investigate the effect of IH on fibroblast activation, we analyzed the expression of α-SMA, collagen I and periostin in the left ventricle of mice after IH exposure. First,
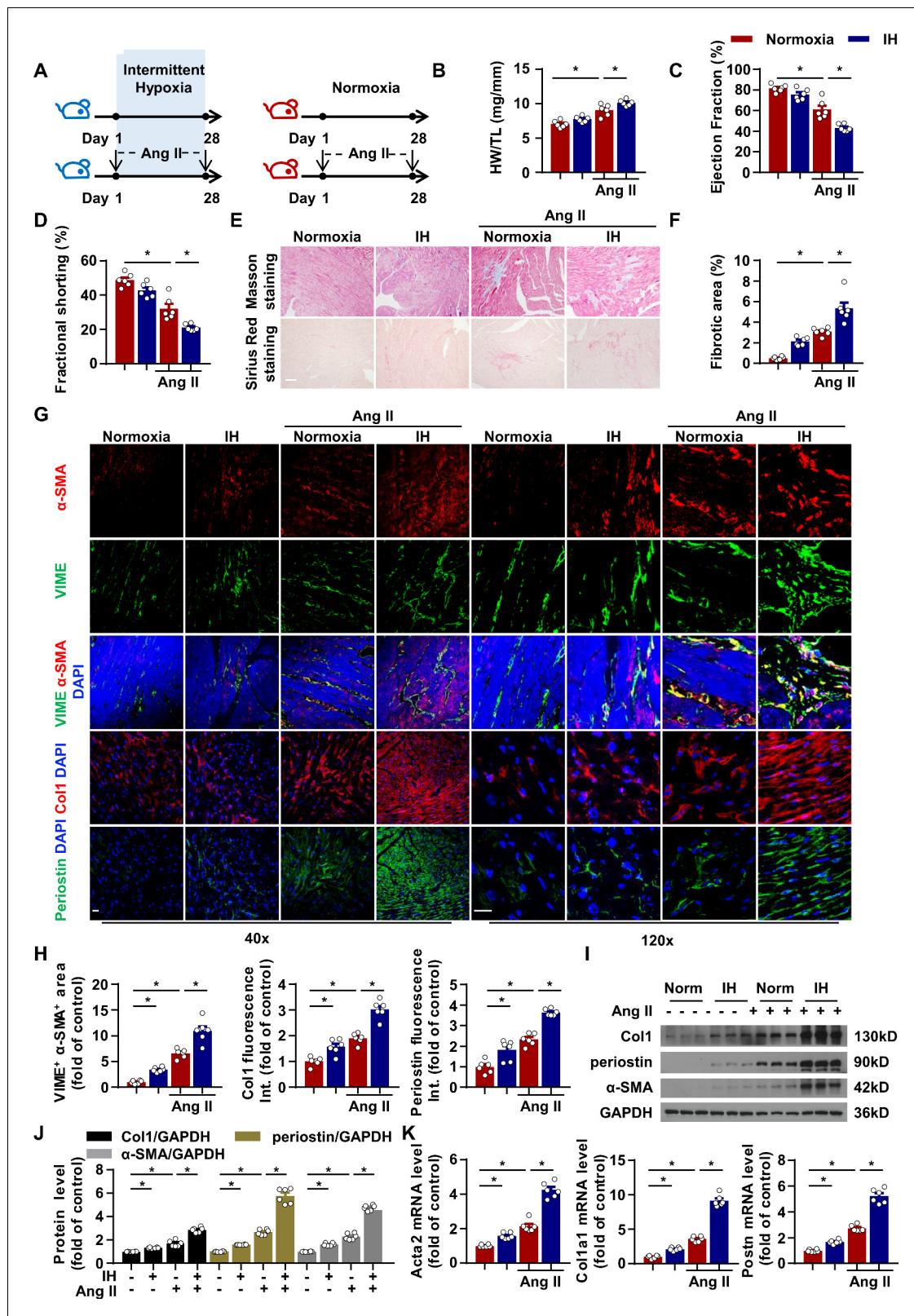
Figure 1. Intermittent hypoxia (IH) induces cardiac fibrosis and aggravates pathological cardiac dysfunction by promoting fibroblast activation in myocardial interstitium. (**A**) C57BL/6 mice were housed under normoxia or IH with or without infusion of angiotensin II (Ang II) for 28 days. (**B**) Ratio of heart weight to tibial length of mice in each group. (**C, D**) Ejection fraction (EF) and fractional shortening (FS) of mice quantified by echocardiography. (**E**) Representative images of Masson and Sirius red staining of left ventricle. Scale bar, 100 μm. (**F**) Quantification of fibrotic area in (**E**). (**G**)

Figure 1 continued on next page

Figure 1 continued

Representative confocal microscopy images of immunofluorescence staining for α-SMA, vimentin (VIME, fibroblast marker), collagen I (Col1), periostin and DAPI. Scale bar, 20 μm. (H) Quantification of co-localization of α-SMA and VIME, Col1 and periostin fluorescence intensity in (G). (I) Col1, periostin, and α-SMA protein level in left ventricle detected by western blot analysis. (J) Quantification of Col1, periostin and α-SMA protein level in (I). (K) Quantification of *Acta2, col1a1* and *Postn* mRNA expression. Data are mean ± SEM, n = 6 mice per group, *p<0.05, 2-way ANOVA with Bonferroni post-test. Data used for quantitative analyses as well as the numerical data that are represented in graphs are available in *Figure 1—source data 1*. The online version of this article includes the following source data and figure supplement(s) for figure 1:

Source data 1. Intermittent hypoxia (IH) induces fibroblast activation and cardiac fibrosis.
Figure supplement 1. The effects of IH on cardiomyocyte morphology and apoptotic status.
Figure supplement 1—source data 1. The effects of IH on cardiomyocyte morphology and apoptotic status.

immunofluorescence staining showed strongly α-SMA signaling in vimentin-positive CFs in the IH group. IH-induced α-SMA expression in CFs was further enhanced under the Ang II-induced cardiac pathologic condition (*Figure 1G–H*). Meanwhile, the expression of collagen I and periostin showed a similar trend as α-SMA expression (*Figure 1G–H*). In addition, IH exposure slightly increased the mRNA and protein levels of α-SMA, collagen I and periostin (*Figure 1I–K*) in the mouse left ventricle and significantly elevated the levels in the left ventricle of Ang II-infused mice (*Figure 1I–K*). These results suggest that IH can activate CFs at the basal level and under the Ang II-induced injury condition.

IH exposure promoted TSP1 expression in CFs

To test whether TSP1 plays an important role in the progression of cardiac fibrosis induced by IH, we next detected TSP1 expression in mice after IH exposure. As compared with normoxia, IH exposure significantly increased plasma TSP1 content and mRNA level in the mouse left ventricle, especially in Ang II-infused mice (*Figure 2A–B*). The protein level of TSP1 in the left ventricle showed a similar trend to that of collagen I and periostin (*Figure 2C–D*). Given that TGFβ and its downstream Smad signaling critically modulate the fibroblast phenotype (*Travers et al., 2016*; *Cucoranu et al., 2005*), we assessed Smad2/3 phosphorylation in the mouse left ventricle. The phosphorylation of Smad2/3 was slightly increased after IH exposure but greatly increased after IH exposure in the Ang II-induced injury condition (*Figure 2C–D*), which is consistent with TSP1 expression. Furthermore, immunofluorescence staining showed elevated signaling of TSP1 in the left ventricle after IH, especially in the Ang II-induced condition (*Figure 2E–F*). In addition, the expression of TSP1 in cells positive for Thy1 (an inclusive surface protein given its association with CFs [*Ali et al., 2014*; *Hudon-David et al., 2007*]) and negative for CD11b (macrophage marker), CD31 (endothelial cell marker), CD45 and Ter119 (hematopoietic cell marker) in the heart, detected by flow cytometry, was significantly higher after IH exposure (*Figure 2G*), which indicated that IH exposure could induce TSP1 expression in CFs.

To identify the potential relevance of TSP1 to OSA, we measured the concentration of TSP1 in plasma samples from 21 patients with OSA and 21 healthy subjects. TSP1 content was significantly increased in patients with OSA as compared with healthy individuals (*Figure 2H*). Together, these data suggest that TSP1 level was elevated in both mice and humans after IH exposure and might contribute to CF activation and cardiac fibrosis.

IH induced primary CF (PCF) activation via TSP1

Next, to confirm the effect of IH on PCF activation in vitro, we used immunofluorescence staining of α-SMA in mouse PCFs (mPCFs) with or without IH exposure. As compared with normoxia, IH increased α-SMA expression in PCFs and led to an activated phenotype of fibroblast cells (*Figure 3A–B*). In addition, IH exposure increased the proliferation and contractility of PCFs (*Figure 3C–D*). We tested whether TSP1 plays an important role in fibroblast activation and found the mRNA expression of *Thbs1* significantly increased by IH as compared with normoxia in mPCFs (*Figure 3E*). In addition, IH significantly increased the protein level of TSP1 beginning from 2 hr and sustained until 8 hr in mPCFs (*Figure 3F–G*). Furthermore, shRNA lentivirus used to produce TSP1 deficiency in PCFs attenuated IH-induced mRNA and protein levels of α-SMA, collagen I and periostin (*Figure 3H–K*). TSP1 deficiency in PCFs also blocked inflammatory gene Tnfa expression
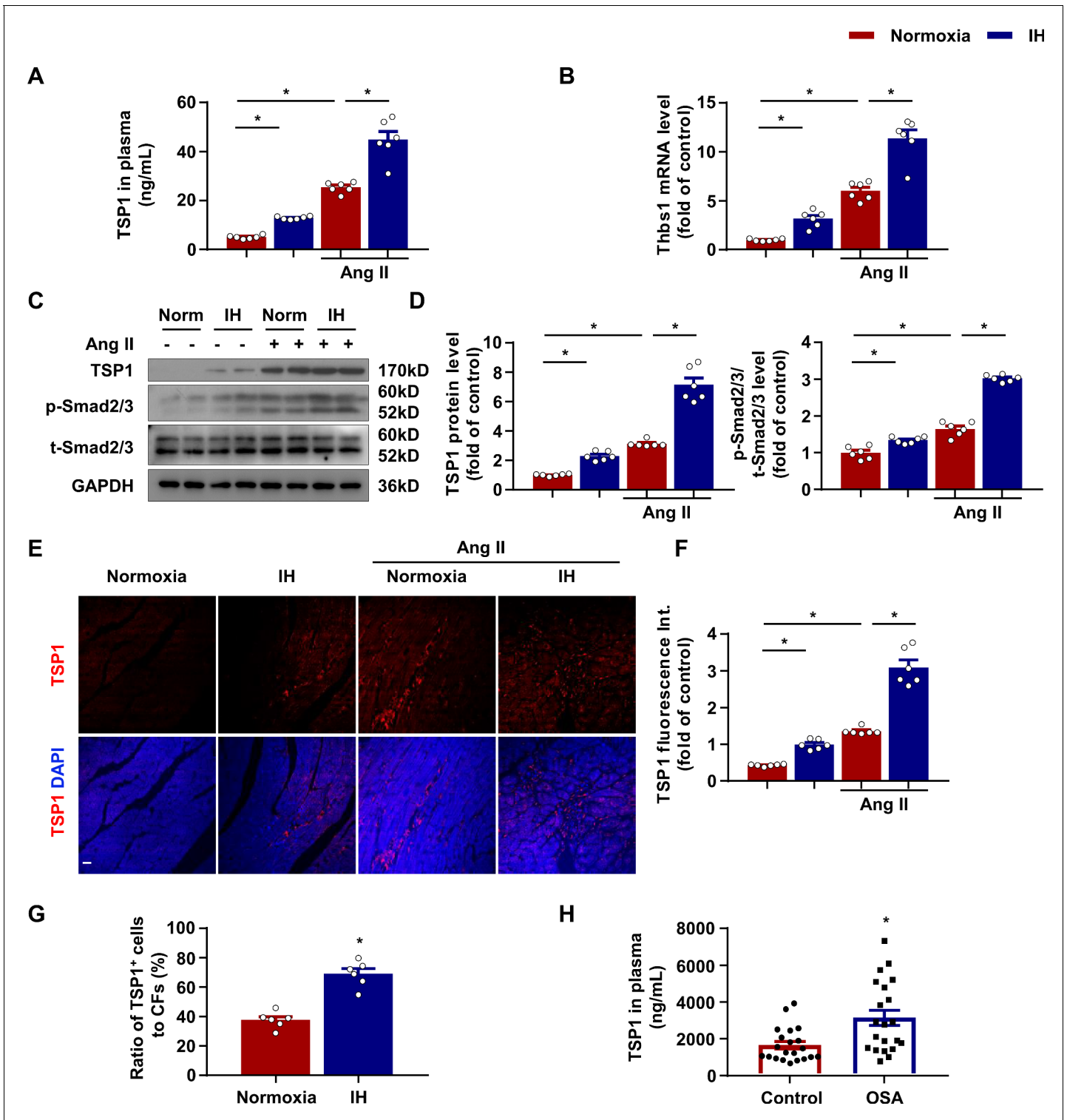
Figure 2. Increased thomsbospondin-1 (TSP1) expression in mice after IH exposure. (**A**) C57BL/6 mice were housed under normoxia or IH with or without infusion of Ang II for 28 days. Plasma concentration of TSP1 in mice detected by ELISA. (**B**) *Thbs1* mRNA level in left ventricle of mice exposed to IH with or without infusion of Ang II for 14 days quantified by RT-PCR. (**C**) C57BL/6 mice were housed under normoxia or IH with or without infusion of Ang II for 28 days. The protein levels of TSP1, phosphorylated Smad2/3 (p-Smad2/3), and total Smad2/3 (t-Smad2/3) in left ventricle of mice detected by western blot analysis. (**D**) Quantification of TSP1 and p-Smad2/3 in (**C**). (**E**) Representative confocal microscopy images of immunofluorescence staining for TSP1 and DAPI. Scale bar, 20 µm. (**F**) Quantification of TSP1 fluorescent intensity in (**E**). Data are mean ± SEM, n = 6 mice per group, *p<0.05, 2-way ANOVA with Bonferroni post-test. (**G**) Quantification of number of cells negative for CD45, CD31, CD11b, and Ter119 and positive for

Figure 2 continued on next page

Figure 2 continued

Thy1 from left ventricle tissue digestion, that stained positive for intracellular TSP1 by flow cytometry. Data are mean ± SEM, n = 6, *p<0.05, unpaired 2-tail *t* test. (H) Plasma concentration of TSP1 in healthy individuals and patients with obstructive sleep apnea (OSA) detected by ELISA. Data are mean ± SEM, n = 21, *p<0.05, unpaired 2-tail *t* test. Data used for quantitative analyses as well as the numerical data that are represented in graphs are available in *Figure 2—source data 1*.

The online version of this article includes the following source data for figure 2:

Source data 1. Intermittent hypoxia (IH) increased thomsbospondin-1 (TSP1) expression.

(*Figure 3I*) induced by IH exposure. Thus, our results suggested that IH induced PCF activation through upregulating TSP1.

IH upregulated phosphorylation of STAT3 at Tyr705 site both in vivo and in vitro

TSP1 was reported to be transcriptionally regulated by STAT3 in astrocytes (*Tyzack et al., 2014*), and emerging evidences has indicated that STAT3 involved in fibrosis diseases (*Chakraborty et al., 2017*; *Wang et al., 2018*). Here, we hypothesized that STAT3 might play a vital role in IH-induced TSP1 expression and cardiac fibrosis. Since the phosphorylation status of STAT3 is related to its transcriptional activity (*Darnell et al., 1994*; *Ihle, 1995*), we determined the phosphorylation of STAT3 at multiple sites as well as the phosphorylation of JAKs in mPCFs under IH. STAT3 phosphorylation at Tyr705 was significantly increased by IH from 0.5 to 2 hr, but STAT3 phosphorylation at Ser727 or total STAT3 was not altered by IH exposure (*Figure 4A–B*). Meanwhile, IH exposure significantly induced the phosphorylation of JAK2 at Tyr1008 without affecting that of JAK1 or JAK3 (*Figure 4A–B*). A JAK2 inhibitor, TG101209, abolished the phosphorylation of STAT3 at Tyr705 induced by IH (*Figure 4C–D*), so IH-induced STAT3 phosphorylation might be mediated by JAK2. Phosphorylation of STAT3 at Tyr705 was reported to be crucial to STAT3 nuclear translocation and transcriptional activity (*Darnell et al., 1994*; *Ihle, 1995*), so we next analyzed the STAT3 subcellular localization. STAT3 nuclear translocation was significantly increased by IH on immunofluorescent staining (*Figure 4E–F*). Moreover, in the mouse left ventricle after IH exposure, consistent with results in vitro, IH exposure induced phosphorylation of STAT3 at Tyr705 but not Ser727 (*Figure 4G–H*). Also, IH exposure or together with Ang II markedly increased STAT3 nuclear localization in vivo (*Figure 4I*). Thus, IH induced STAT3 activation via JAK2-mediated STAT3 phosphorylation at Tyr705.

STAT3 silencing or inhibition blunted IH-induced TSP1 expression and CF activation

We next explored the role of STAT3 in IH-induced TSP1 expression and CF activation. Knockdown of STAT3 with siRNA almost completely abolished IH-induced TSP1 expression both in mRNA and protein level (*Figure 5A–C*). Simultaneously, IH-induced α-SMA, collagen I and periostin expression was blocked by STAT3 knockdown at both the mRNA and protein level (*Figure 5A–C*). To further assess the importance of STAT3 transcriptional activity, we treated PCFs with S3I-201, a selective STAT3 inhibitor. S3I-201 barely showed effect on the basal level of TSP1, α-SMA, collagen I and periostin expression but significantly attenuated IH-induced expression of TSP1, α-SMA, collagen I and periostin at both the mRNA and protein level (*Figure 5D–F*). Quantitative chromatin immunoprecipitation (ChIP) assay proved that IH enhanced the enrichment of STAT3 at TSP1 promoter in PCFs as compared with the control (*Figure 5—figure supplement 1A*). Taken together, our results indicated a predominant role of STAT3 in IH-induced CF activation.

Pharmacological or genetic inhibition of STAT3 ameliorates IH-induced cardiac dysfunction and fibrosis

As we found that STAT3-induced TSP1 contributed to IH-induced CF activation, we injected S3I-201 into IH-exposed mice with or without Ang II infusion for 28 days (*Figure 6A*). First, echocardiography analysis showed that S3I-201 promoted significant recovery of ratio of heart weight to tibial length (*Figure 6B*) and EF after IH exposure (*Figure 6C*). Moreover, on Masson staining, S3I-201 reduced IH-induced fibrosis under both basal and Ang II infusion conditions (*Figure 6D–E*). In addition, immunofluorescence staining showed significantly decreased TSP1, collagen I, periostin and α-SMA
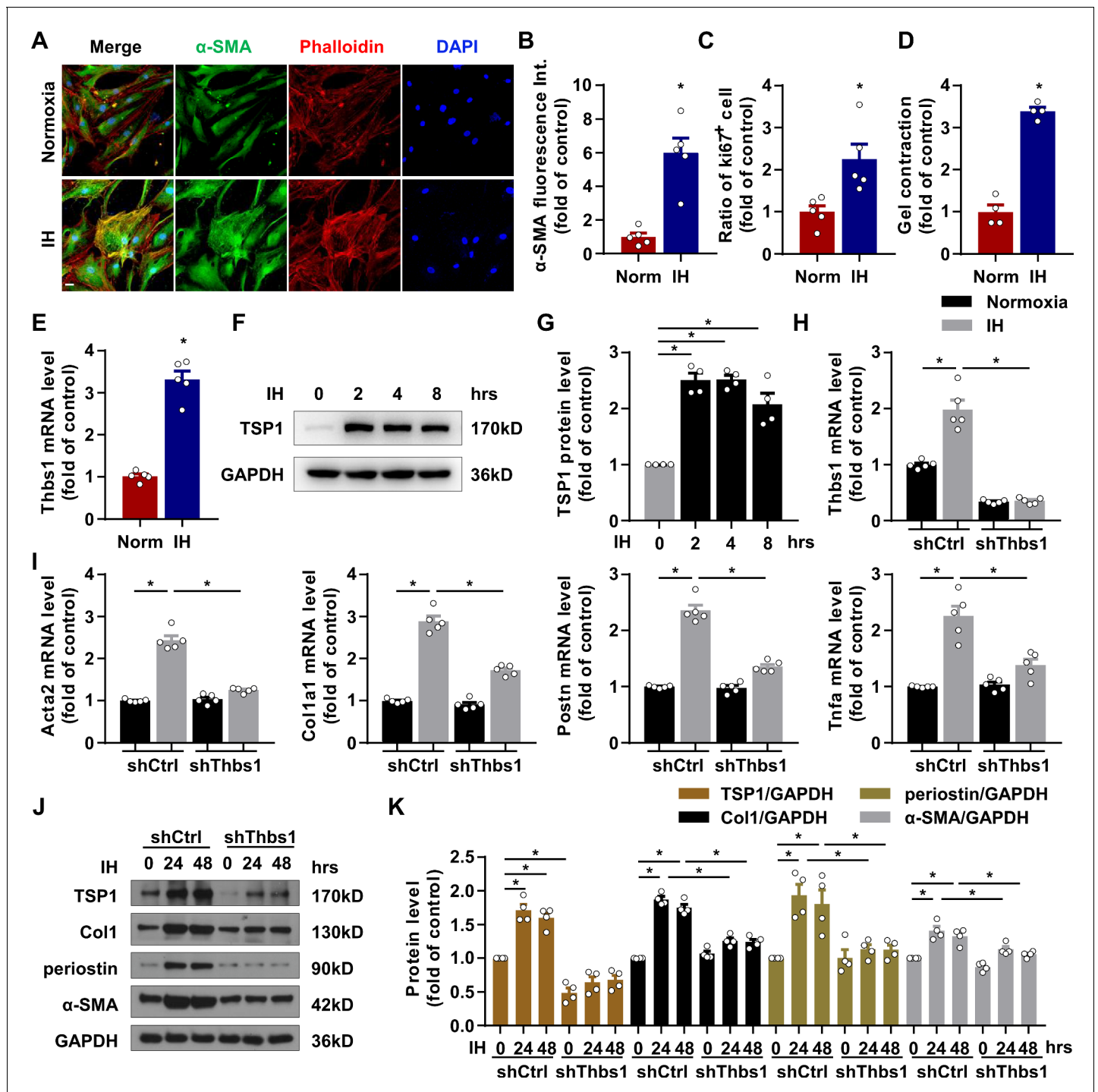
Figure 3. IH induced cardiac fibroblast (CF) activation via TSP1. (**A**) Mouse primary CFs (mPCFs) were cultured under normoxia or IH for 24 hr. Representative confocal microscopy images of immunofluorescence stained for α-SMA, phalloidin and DAPI. Scale bar, 20 μm. (**B**) α-SMA fluorescence intensity quantification. (**C**) Ratio of Ki67 positive cells to total mPCFs after IH exposure for 24 hr. Data are mean ± SEM, n = 5 independent experiments, *p<0.05, unpaired 2-tail *t* test. (**D**) Quantification of gel contraction by mPCFs after IH exposure for 24 hr. Data are mean ± SEM, n = 4 independent experiments, *p<0.05, unpaired 2-tail *t* test. (**E**) *Thbs1* mRNA levels detected by RT-PCR. Data are mean ± SEM, n = 5 independent experiments, *p<0.05, unpaired 2-tail *t* test. (**F**) Expression of TSP1 in mPCFs exposed to IH for the indicated time detected by western blot analysis. (**G**) Quantification of TSP1 in (**F**). Data are mean ± SEM, n = 4 independent experiments, *p<0.05, 1-way ANOVA with Bonferroni post-test. (**H–K**) mPCFs were infected with lentivirus to deliver Thbs1 shRNA (LV-shThbs1) or control shRNA (LV-shCtrl) for 48 hr, then cultured under normoxia or IH for 24 hr. (**H–I**) *Thbs1, Acta2, Col1a1, Postn* and *Tnfa* mRNA levels detected by RT-PCR. Data are mean ± SEM, n = 5 independent experiments, *p<0.05, 2-way ANOVA with Bonferroni post-test. (**J**) Protein level of TSP1, collagen I (Col1), periostin and α-SMA detected by western blot analysis. (**K**) Quantification

Figure 3 continued on next page

Figure 3 continued

of TSP1, Col1, periostin and α-SMA in J). Data are mean ± SEM, n = 4 independent experiments, *$p<0.05$, 2-way ANOVA with Bonferroni post-test. Data used for quantitative analyses as well as the numerical data that are represented in graphs are available in *Figure 3—source data 1*.

The online version of this article includes the following source data for figure 3:

Source data 1. Intermittent hypoxia (IH) induced cardiac fibroblast (CF) activation.

expression in the mouse left ventricle after S3I-201 treatment under both basal and Ang II infusion conditions (*Figure 6D–E*). The expression of TSP1, collagen I, periostin and α-SMA, as well as phosphorylation of STAT3 at Tyr705 site in the left ventricle showed similar trends (*Figure 6F–G*).

To further investigate whether S3I-201 could reverse the damage already induced by IH, we treated mice with S3I-201 for 2 weeks after exposure to IH and Ang II for 28 days (*Figure 6—figure supplement 1A*). The ratio of heart weight to tibial length, EF and fibrotic area in mice were comparable between groups (*Figure 6—figure supplement 1B–E*). In addition, because systemic S3I-201 administration might protect the heart via direct and indirect mechanisms, we determined the effect of AAV9-periostin promoter-shStat3 on IH-induced fibrosis (*Figure 6—figure supplement 1F*). Evidence from flow cytometry confirmed the knockdown of STAT3 in CFs (*Figure 6—figure supplement 1G*). Similar to that observed in animals subjected to S3I-201 treatment, AAV9-periostin promoter-shStat3 promoted a significant recovery of ratio of heart weight to tibial length and EF after IH exposure (*Figure 6—figure supplement 1H–I*), and reduced IH-induced fibrosis under both basal and Ang II infusion conditions (*Figure 6—figure supplement 1J–K*). These results suggest that pharmacological or genetic inhibition of STAT3 might be a potential therapeutic strategy for cardiac fibrosis induced by IH.

Discussion

In the last decades, we have extensive evidence for a causal link between OSA and cardiovascular disease (*Gozal and Kheirandish-Gozal, 2008*). Here, we provide definitive evidence of elevated plasma TSP1 level in both humans with OSA and mice exposed to IH. Moreover, we found that TSP1 activated TGFβ signaling, which subsequently promoted the transformation of CFs to myofibroblasts, dependent on STAT3 Tyr705 phosphorylation. Finally, pharmacological inhibition of STAT3 with S3I-201 or AAV9-periostin promoter-shStat3 significantly attenuated IH-induced cardiac fibrosis under both basal and Ang II infusion conditions (*Figure 6H*).

TSP1 belongs to the thrombospondin family, a conserved family of extracellular, oligomeric, multidomain, calcium-binding glycoproteins that can be secreted by various cell types (*Crawford et al., 1998*; *Adams and Lawler, 2011*; *Hugo et al., 1998*). Increased TSP1 levels are associated with many kinds of cardiovascular diseases, including pulmonary hypertension (PH), idiopathic interstitial pneumonia and aging (*Ide et al., 2008*; *van Almen et al., 2011*; *Kaiser et al., 2016*; *Kumar et al., 2017*; *Rogers et al., 2017*). In individuals with end-stage PH, both protein and mRNA levels of TSP1 are elevated in the lung parenchyma and pulmonary artery (*Rogers et al., 2017*). Furthermore, TSP1 blockade protected against Schistosoma- and hypoxia-induced PH (*Kumar et al., 2017*). In our study, TSP1 protein expression was significantly elevated in patients with OSA as compared with healthy controls. Strikingly, OSA incidence is high in patients with PH, idiopathic pulmonary fibrosis, and other cardiac diseases, which suggests that TSP1 might be the common pathologic mechanism in OSA-associated cardiovascular diseases. Therefore, TSP1 might be a biomarker for diagnosis of OSA-related cardiac dysfunction, and reducing IH-upregulated TSP1 expression might be crucial to protect the cardiac function of patients with sleep apnea.

TGFβ, perhaps the most extensively studied mediator of fibroblast activation and having the greatest role in pathological fibrosis (*Travers et al., 2016*; *Leask and Abraham, 2004*), can be activated by TSP1 binding to a defined site on latency-associated propeptide and inducing a conformational change in the latent complex (*Murphy-Ullrich and Poczatek, 2000*; *Ribeiro et al., 1999*). The kinetics of its gene expression, along with its independence from de novo protein synthesis, led to classifying TSP1 as an immediate early-response gene (*Majack et al., 1987*; *Patel et al., 1997*). For example, in vascular smooth muscle cells, the mRNA level of TSP1 was induced rapidly within 15 min by platelet-derived growth factor (*Majack et al., 1987*). Consistently, we found that IH upregulated *Thbs1* continuously from 2 to 8 hr. However, IH-induced TSP1 protein expression in PCFs peaked at
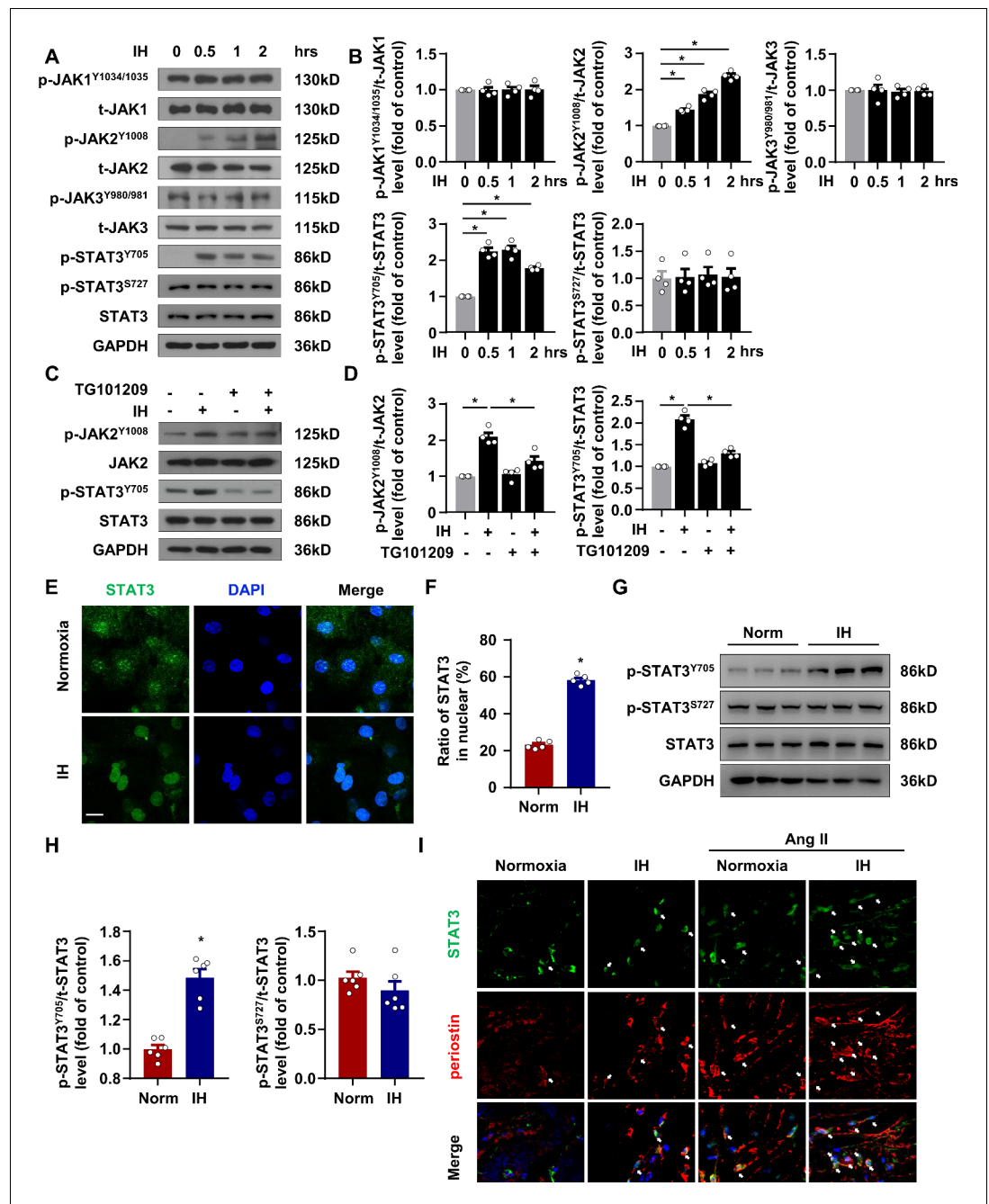
Figure 4. IH induced STAT3 signaling activation in CFs. (**A**) mPCFs were cultured and exposed to IH for the indicated time. The protein levels of phosphorylated JAK1 at Tyr1034/1035 (p-JAK1$^{Y1034/1035}$), total JAK1 (t-JAK1), p-JAK2 at Tyr1008 (p-JAK2^{Y1008}), total JAK2 (t-JAK2), p-JAK3 at Tyr980/981 (p-JAK3$^{Y980/981}$), total JAK3 (t-JAK3), p-STAT3 at Tyr705 (p-STAT3^{Y705}) and Ser727 (p-STAT3^{S727}) and total STAT3 (t-STAT3) detected by western blot analysis. (**B**) Quantification of indicated protein levels in (**A**). Data are mean ± SEM, n = 4 independent experiments, *p<0.05, 1-way ANOVA with Bonferroni post-test. (**C–D**) mPCFs were cultured and exposed to IH for 1 hr with or without TG101209 (2 μM). Indicated protein levels were analyzed (**D**). (**E**) mPCFs were exposed to IH for 1 hr. Representative confocal microscopy images of immunofluorescence staining for STAT3 and DAPI. Scale bar, 20 μm. (**F**) Quantification of subcellular localization of STAT3 in (**E**). Data are mean ± SEM, n = 5 independent experiments, *p<0.05, unpaired 2-tail *t* test. (**G**) The protein levels of p-STAT3^{Y705} and p-STAT3^{S727} in ventricles of mice with or without IH detected by western blot analysis. (**H**) Quantification of p-STAT3^{Y705}, p-STAT3^{S727} and t-STAT3 in (**E**). Data are mean ± SEM, n = 6 mice per group, *p<0.05, unpaired 2-tail *t* test. (**I**) Representative confocal microscopy images of immunofluorescence staining for STAT3, periostin, and DAPI in mice exposed IH

Figure 4 continued on next page

Figure 4 continued

with or without Ang II infusion for 4 weeks. The white arrows indicate periostin-positive cells with nuclear localization of STAT3. Scale bar, 10 μm. Data used for quantitative analyses as well as the numerical data that are represented in graphs are available in *Figure 4—source data 1*.

The online version of this article includes the following source data for figure 4:

Source data 1. Intermittent hypoxia induced STAT3 signaling activation.

2 hr and decreased from 4 to 8 hr. The concentration of TSP1 in culture medium was still increased from 4 to 8 hr, which suggests that IH might promote TSP1 secretion as well. However, the mechanism underlying TSP1 secretion needs further elucidation.

STAT3, as a multifaceted molecule, plays a central role in organic fibrogenesis and cardiac hypertrophy (*Su et al., 2017*). Hypoxic stress can induce phosphorylation of STAT3 and its simultaneous nuclear translocation (*Noman et al., 2009*). Here we found that STAT3, as a TSP1 transcription factor, was phosphorylated at Tyr705 and translocated into the nucleus after IH exposure, then promoted fibroblast activation. In addition, STAT3-null mice showed severe fibrosis with age (*Jacoby et al., 2003*), but in transaortic constriction-induced cardiac remodeling, selective inhibition of STAT3 by S3I-201 significantly improved EF and decreased the left ventricle chamber dilation (*Unudurthi et al., 2018*). Consistently, we found that S3I-201 treatment reduced the pathologic upregulation of TSP1 and ameliorated the cardiac fibrosis of IH-exposed mice with or without Ang II infusion. Importantly, these results were further confirmed by using AAV9-periostin promoter-shStat3. Direct blockade of TSP1/TGFβ signaling is a major therapeutic challenge because of its ubiquitous nature and localized signaling effects (*Kumar et al., 2017*). Our results indicated that targeting the pathologic activation of STAT3 might hold promise as a potentially safe approach in preventing IH-induced cardiac fibrosis.

In summary, our study demonstrated that IH upregulated the expression of TSP1 in both mice and humans, and TGFβ pathway activation induced by JAK2/STAT3/TSP1 signaling played a vital role in IH-induced fibroblast activation and cardiac fibrosis. Pharmacological or genetic inhibition of STAT3 might be a potential therapeutic strategy in managing several diverse yet intertwined human pathologies related to IH.

Materials and methods

Key resources table

Reagent type (species) or resource	Designation	Source or reference	Identifiers	Additional information
Antibody	anti-thrombospondin-1 (Rabbit monoclonal)	Cell Signaling Technology	Cat# 37879	WB (1:1000)
Antibody	anti-phospho-SMAD2/3 (Rabbit monoclonal)	Cell Signaling Technology	Cat# 8828	WB (1:1000)
Antibody	anti-SMAD2/3 (Rabbit monoclonal)	Cell Signaling Technology	Cat# 8685	WB (1:1000)
Antibody	anti-phospho-JAK1 (Rabbit monoclonal)	Cell Signaling Technology	Cat# 74129	WB (1:1000)
Antibody	anti-phospho-JAK2 (Rabbit monoclonal)	Cell Signaling Technology	Cat# 8082	WB (1:1000)
Antibody	anti-phospho-JAK3 (Rabbit monoclonal)	Cell Signaling Technology	Cat# 5031	WB (1:1000)
Antibody	anti-JAK1 (Rabbit monoclonal)	Cell Signaling Technology	Cat# 3344	WB (1:1000)
Antibody	anti-JAK2 (Rabbit monoclonal)	Cell Signaling Technology	Cat# 3230	WB (1:1000)
Antibody	anti-JAK3 (Rabbit monoclonal)	Cell Signaling Technology	Cat# 8827	WB (1:1000)

Continued on next page

Continued

Reagent type (species) or resource	Designation	Source or reference	Identifiers	Additional information
Antibody	anti-phospho-STAT3 (Tyr705) (Rabbit monoclonal)	Cell Signaling Technology	Cat# 9145	WB (1:1000)
Antibody	anti-phospho-STAT3 (Ser727) (Rabbit polyclonal)	Cell Signaling Technology	Cat# 9134	WB (1:1000)
Antibody	anti-STAT3 (Rabbit monoclonal)	Cell Signaling Technology	Cat# 12640	WB (1:1000) ChIP (1:50)
Antibody	anti-STAT3 (Mouse monoclonal)	Cell Signaling Technology	Cat# 9139	IF (1:100) FACS (1 µL per test)
Antibody	Normal Rabbit IgG	Cell Signaling Technology	Cat# 2729	ChIP (1 µg per test)
Antibody	anti-thrombospondin antibody (Mouse monoclonal)	Abcam	Cat# ab1823	IF (1:50) FACS (1 µL per test)
Antibody	anti-αSMA (Mouse monoclonal)	Abcam	Cat# ab7817	WB (1:1000) IF (1:100)
Antibody	anti-Collagen I antibody (Mouse monoclonal)	Abcam	Cat# ab6308	WB (1:1000) IF (1:100)
Antibody	anti-periostin (Rabbit polyclonal)	Abcam	Cat# ab14041	WB (1:1000) IF (1:100)
Antibody	anti-vimentin (Rabbit monoclonal)	Abcam	Cat# ab92547	IF (1:500)
Antibody	anti-GAPDH (Mouse monoclonal)	Proteintech	Cat# 60004	WB (1:1000)
Antibody	anti-Ki67 (Rabbit monoclonal)	HuaAn Biotechnology Co	Cat# ET1609-34	IF (1:100)
Antibody	anti-mouse CD45-PE Cy7 (Rat monoclonal)	BioLegend	Cat# 103114	FACS (1 µL per test)
Antibody	anti-mouse CD31-PE Cy7 (Rat monoclonal)	BioLegend	Cat# 102523	FACS (1 µL per test)
Antibody	anti-mouse CD11b-PE Cy7 (Rat monoclonal)	BioLegend	Cat# 101215	FACS (1 µL per test)
Antibody	anti-mouse Ter119-PE Cy7 (Rat monoclonal)	BioLegend	Cat# 116221	FACS (1 µL per test)
Antibody	anti-mouse thy1- Alexa Fluor 488 (Mouse monoclonal)	BioLegend	Cat# 202505	FACS (1 µL per test)
Antibody	anti-mouse thy1- Alexa Fluor 488 (Rat monoclonal)	BioLegend	Cat# 105315	FACS (1 µL per test)
Antibody	PE RAT anti-mouse IgG1	BD Biosciences	Cat# 550083	FACS (1 µL per test)
Antibody	Alex 594-conjugated goat anti-mouse antibody	Thermo Fisher Scientific	Cat# A-11005	IF (1:200)
Antibody	Alex 488-conjugated goat anti-rabbit antibody	Thermo Fisher Scientific	Cat# A-11008	IF (1:200)
Sequence-based reagent	Stat3 siRNA	Santa Cruz Biotechnology	Cat# sc-29494	
Sequence-based reagent	Control siRNA	Santa Cruz Biotechnology	Cat# sc-37007	
Sequence-based reagent	Mouse Acta	This paper	N/A	Sequences in *Supplementary file 1*
Sequence-based reagent	Mouse Col1a1	This paper	N/A	Sequences in *Supplementary file 1*

Continued on next page

Continued

Reagent type (species) or resource	Designation	Source or reference	Identifiers	Additional information
Sequence-based reagent	Mouse Postn	This paper	N/A	Sequences in *Supplementary file 1*
Sequence-based reagent	Mouse Thbs1	This paper	N/A	Sequences in *Supplementary file 1*
Sequence-based reagent	Mouse Tnfa	This paper	N/A	Sequences in *Supplementary file 1*
Sequence-based reagent	Mouse Stat3	This paper	N/A	Sequences in *Supplementary file 1*
Sequence-based reagent	Mouse 18S	This paper	N/A	Sequences in *Supplementary file 1*
Peptide, recombinant protein	Angiotensin II	Abcam	Cat# ab120183	
Commercial assay or kit	TSP1 ELISA KIT(Human)	R and D Systems	Cat# DTSP10	
Commercial assay or kit	TSP1 ELISA KIT(Mouse)	Cloud-Clone Corp.	Cat# SEA611Mu	
Commercial assay or kit	TUNEL staining kit	KeyGEN BioTECH	Cat# KGA7073-1	
Commercial assay or kit	SimpleChIP Enzymatic Chromatin IP Kit	Cell Signaling Technology	Cat# 9003	
Commercial assay or kit	Eastep Super Total RNA Extraction Kit	Promega Corporation	Cat# LS1040	
Chemical compound, drug	S3I-201	Santa Cruz Biotechnology	Cat# sc-204304	
Chemical compound, drug	TG101209	MedChem Express	Cat# HY-10410	
Software, algorithm	Prism version 7.0	GraphPad Software Inc	https://www.graphpad.com/scientific-software/prism/	
Software, algorithm	ImageJ version 1.52a	NIH	https://imagej.nih.gov/ij/	
Software, algorithm	FlowJo version 10	Tree Star Inc	https://www.flowjo.com/solutions/flowjo/downloads	

Animals

Male C57BL/6J mice at 8–10 weeks of age were used. All mice were housed in a controlled environment (20 ± 2℃, 12 hr/12 hr light/dark cycle) and maintained on a standard chow diet with free access to water. Intermittent hypoxia (IH) was induced as described previously by using an automated system to control ambient oxygen concentration (*Savransky et al., 2007*; *Chen et al., 2005*). Briefly, O_2 concentration was decreased to 4–6% approximately every 60 s. IH mice were exposed to IH for 8 hr/day in the light time for 28 days. In the pathologic cardiac fibrosis model, mice were subcutaneously implanted with an osmotic minipump (2004 model, Alzet, CA) containing Ang II (1 mg/kg/day) in saline (0.9% w/v) or an identical volume of saline. After the surgery, all mice were exposed to IH for 28 days. In rescue experiments, S3I-201 (5 mg/kg) was given by intraperitoneal injection every 2 days during or after the IH exposure.

Adeno-associated virus (AAV) construction and infection

The AAV used in this study was constructed as previously reported (*Piras et al., 2016*). Briefly, AAV9 carrying a periostin promoter driving the expression of shRNA targeting Stat3 (AAV9-periostin promoter-shStat3) was constructed by Shanghai Genechem Co. (Shanghai). The sequences of the shRNAs were for shStat3, GTCACACAGATGAACTTGGTCTTCAGGT and GCATCAATCCTGTGGTATA. The periostin AAV9-periostin promoter-shStat3 or AAV9-periostin promoter-shScramble
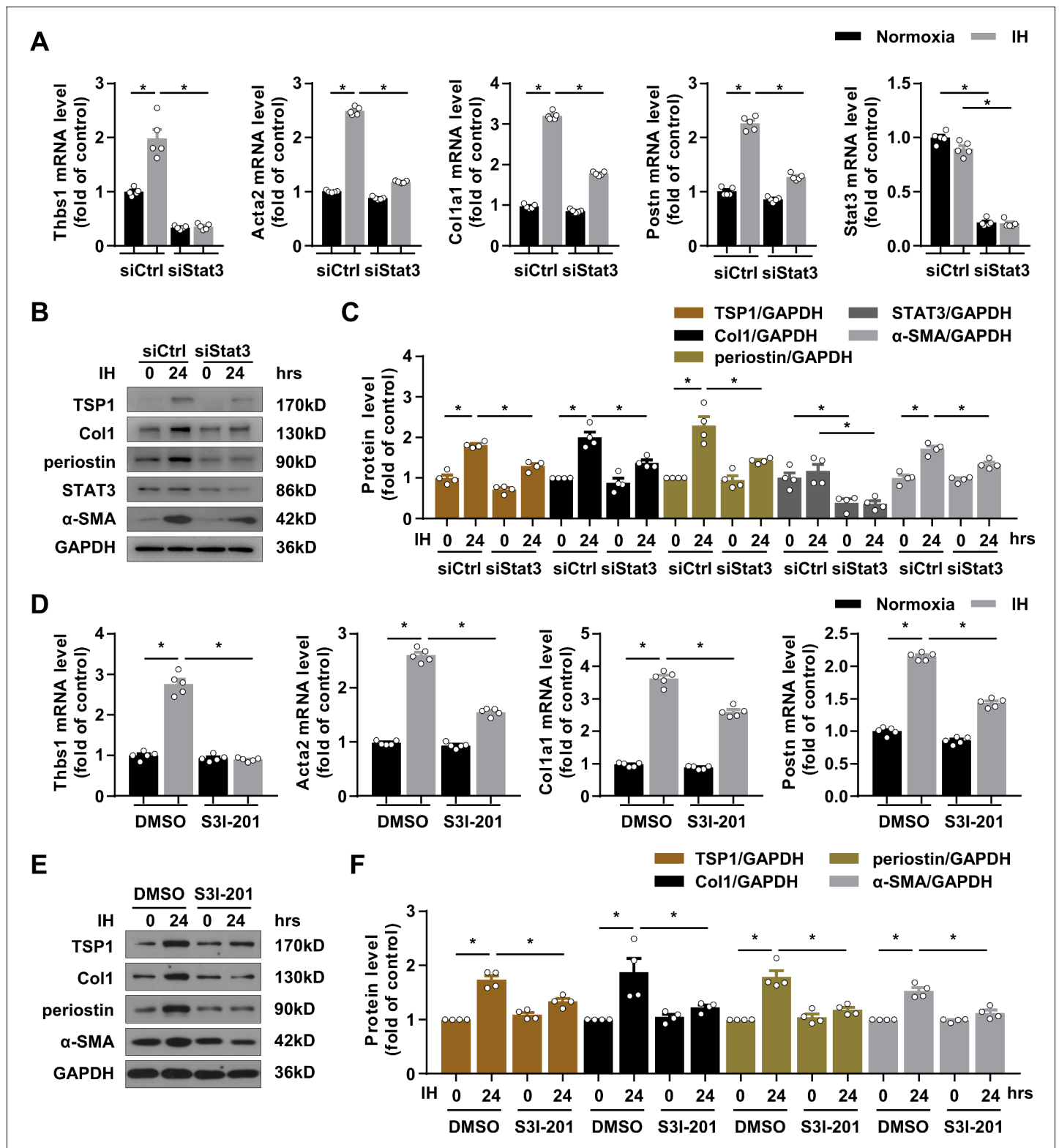
Figure 5. Silencing and inactivating STAT3 downregulated TSP1 expression and attenuated IH-induced CF activation. (A–C) mPCFs were transduced with STAT3 siRNA (siSTAT3) or control siRNA (siCtrl) for 24 hr, then cultured under normoxia or IH for 24 hr. (A) *Thbs1*, *Acta2*, *Col1a1*, *Postn*, *Stat3* mRNA levels were quantified by RT-PCR. Data are mean ± SEM, n = 5 independent experiments, *p<0.05, 2-way ANOVA with Bonferroni post-test. (B) The protein levels of TSP1, collagen I (Col1), periostin, STAT3 and α-SMA detected by western blot analysis. (C) Quantification of TSP1, Col1, periostin, STAT3 and α-SMA protein level in (B). Data are mean ± SEM, n = 4 independent experiments, *p<0.05, 2-way ANOVA with Bonferroni post-test. (D–F)
Figure 5 continued on next page

$(1.5 \times 10^{11} \text{ v.g})$ was injected into the tail vein of mice. At 1 week post-injection, mice were exposed to IH with or without Ang II infusion.

Echocardiography

Trans-thoracic echocardiography was performed on all mice by using a Vevo 2100 system with a MS400 linear array transducer (VisualSonics, ON, Canada) as previously reported (*Zhang et al., 2018*). Briefly, mice were anesthetized with 2% isoflurane and kept warm on a heated platform (37° C). The chest hairs were removed by using depilatory cream, and a layer of acoustic coupling gel was applied to the thorax. An average of 10 cardiac cycles of standard 2-D and m-mode short axis at mid-papillary muscle level were analyzed. Left ventricular ejection fraction and dimensions were calculated by using a modified Quinone method.

Histology

Tissues were fixed in 10% neutral-buffered formalin for 24 hr at room temperature and embedded in paraffin. Hearts were sectioned at 5 μm for staining. Collagen deposition was stained with Masson's trichrome (Sigma-Aldrich, MO) and Sirius red (Solarbio Life Sciences, Beijing) according to the manufacturer's instructions. Images of sections were captured under an Olympus inverted microscope (IX53, Tokyo) and fibrotic areas were semi-quantitatively determined by using ImageJ 1.52.

For immunofluorescence staining, harvested hearts were fixed and embedded in OCT (VWR, PA) and sectioned at 5 μm. Then, sections were stained with primary antibodies for TSP1, Collagen I, periostin, α-SMA and vimentin overnight at 4°C. Alex 488-conjugated goat anti-rabbit and Alex 594-conjugated goat anti-mouse antibodies were used as secondary antibodies. Nuclei were stained with DAPI. TUNEL staining kit (KGA7073-1, KeyGEN BioTECH, Nanjing) was used for analyzing apoptotic cells in cardiac tissue. Images were acquired under an Olympus inverted microscope (IX81, Tokyo). Fluorescent intensity was quantified by using ImageJ. Colocalization of α-SMA and vimentin was quantified by using the Image J with colocalization plugin. Briefly, the plugin initially generates an 8-bit image with only the colocalized points, then it combines the three 8-bit images in an RGB image. Two points are considered as colocalized if their respective intensities are strictly higher than the threshold of their channels.

RT–qPCR

RNA was extracted by using the Eastep Super Total RNA Extraction Kit (LS1040, Promega, WI). cDNA was synthesized by using the iScript cDNA Synthesis Kit (Bio-Rad, CA). Quantitative RT-PCR was performed with gene-specific primers shown in *Supplementary file 1*.

Western blot analysis

Proteins were isolated from snap-frozen heart tissue and cultured cardiac fibroblasts (CFs), which were extracted in RIPA solution with a protease inhibitor cocktail (#4693132001) and PhosSTOP (#04906845001, both Roche, IN). Proteins were quantified by using the BCA Protein Assay Kit (Thermo Fisher Scientific, MA). Then, 20 μg each protein was separated on SDS-PAGE and electro-transferred onto PVDF membranes, blocked with TBST containing 5% bovine serum albumin, and blots on membranes incubated with antigen and antibody complexes were detected by an ECL
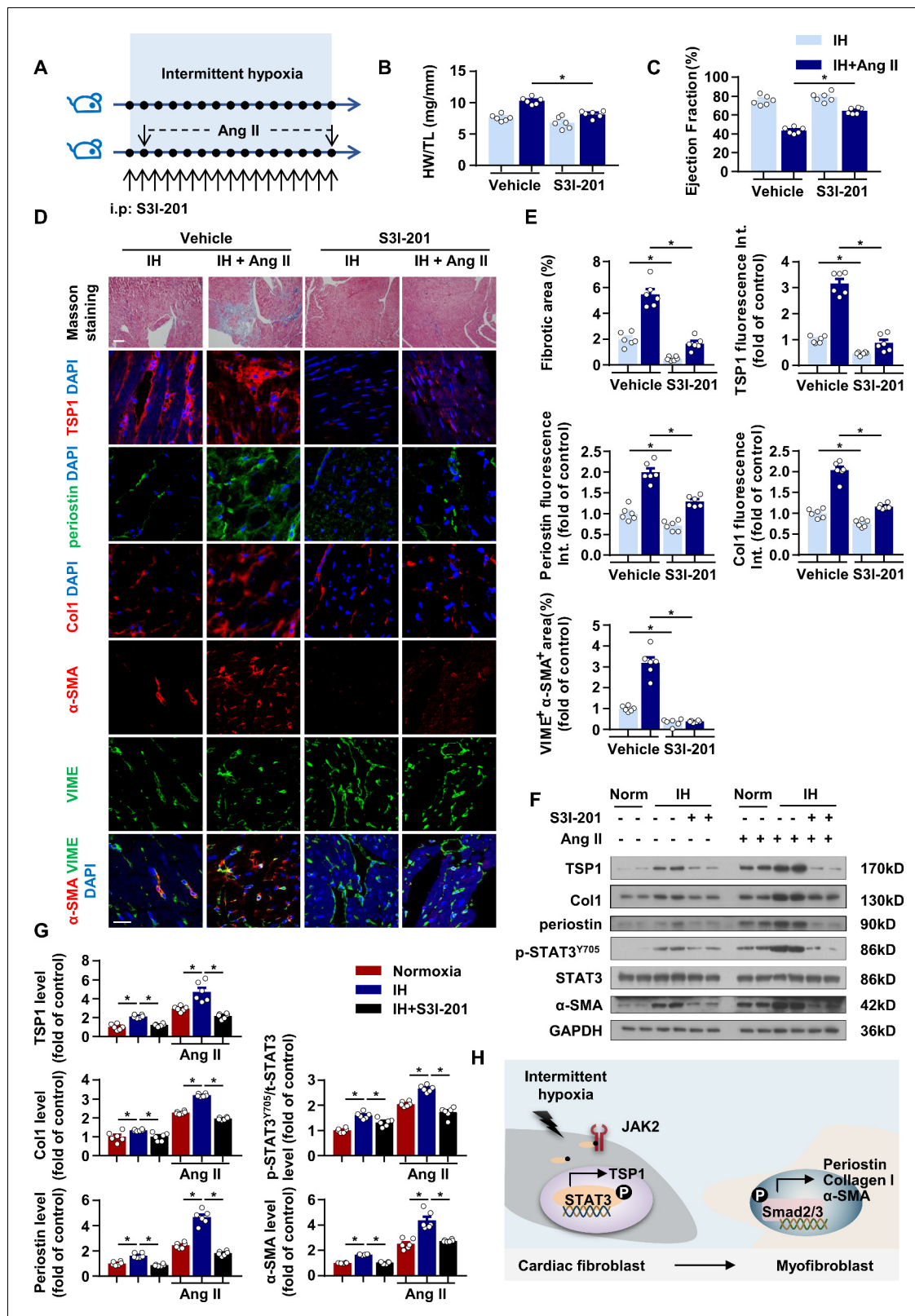
Figure 6. STAT3 inhibitor ameliorated IH-induced cardiac fibrosis. (**A**) C57BL/6 mice exposed to IH with or without infusion of Ang II were treated with S3I-201 or vehicle. (**B**) Ratio of heart weight to tibial length of mice. (**C**) Quantification of ejection fraction (EF) after echocardiography of mice. (**D**) Representative Masson staining of left ventricle of mice. Immunofluorescence staining of left ventricle for TSP1, periostin, Collagen I (Col1), α-SMA, VIME and DAPI. Scale bar, 100 μm. (**E**) Quantification of fibrotic area in Masson-stained slides (**D**), quantification of TSP1, periostin, and Col1 fluorescent

Figure 6 continued on next page

protocol with horseradish peroxidase-conjugated IgG as secondary antibodies. Immunoblots were quantified by using ImageJ 1.52.

Isolation and culture of primary CFs (PCFs)

Isolation of mouse primary CFs (mPCFs) was performed as previously reported (*Su et al., 2017*). Briefly, mouse hearts from freshly euthanized C57BL/6 mice were harvested and minced to 1 mm (*Somers et al., 2008*) in cold phosphate buffered saline. Minced tissue was subsequently digested with buffer containing collagenase II (#V900892, Sigma-Aldrich, MO) and trypsin (Solarbio life Sciences, Beijing) under constant stirring at 37°C for 60 min. The supernatants were spun to collect cells. Then cells resuspended in DMEM/F12 (#11320033, Gibco, MA) were plated into dishes and incubated for 2 hr. Supernatant was discarded and dishes were replenished with fresh medium. mPCFs were incubated at 37°C in a humidified atmosphere of 5% CO_2 and grown to 70–80% confluence. Cells at passages 2 to 3 were used in experiments. Cells exposed to IH were maintained in a hypoxia chamber (5% CO_2; balance N_2 and O_2 from 5% to 21%) for the indicated times.

Flow cytometry

Flow cytometry was performed as previously reported (*Ali et al., 2014*). Digested cells from mouse hearts were suspended in staining buffer containing the relevant surface marker antibodies (PE/Cy7 anti-mouse CD45, CD31, CD11b, Ter119, and Alexa Fluor 488 anti-mouse Thy1) in the dark for 30 min at room temperature. Then, for intracellular staining, cells were fixed with cold methanol for 10 min at −20°C, then incubated with a stain buffer containing TSP1 or STAT3 antibody. After three washing steps, a secondary antibody conjugated to PE was added. The cells were then washed and ready for analysis.

Cell immunofluorescence staining

Mouse primary CFs were fixed with 4% paraformaldehyde and permeabilized with 0.25% Triton X-100. Then cells were stained with antibodies against α-SMA (1:100), STAT3 (1:100) or Ki67 (1:100). Alexa Fluor antibodies (1:200) were used as secondary antibodies. Stress fibers were stained with rhodamine phalloidin (Thermo Fisher Scientific, MA). Nuclei were stained with DAPI. Images were acquired under an Olympus laser scanning microscope (IX81, Tokyo).

Collagen gel contraction assay

The collagen contraction assay was performed as previously reported (*Pincha et al., 2018*). Mouse primary CFs were embedded in collagen gel containing collagen type I from rat tail (#08–115, Sigma-Aldrich, MO) and culture medium. Contraction was measured from the gel images after 24 hr.

Lentivirus construction and infection

Lentiviruses carrying short hairpin (shRNA) for *Thbs1* (LV-shThbs1) and non-specific shRNA (LV-shCtrl) were constructed by Shanghai Genechem Co. (Shanghai). CFs were infected with lentivirus at multiplicity of infection (MOI) 10, and no detectable cellular toxicity was observed.

ELISA

The secretion of TSP1 in mice or human plasma was quantified by using an ELISA kit (SEA611Mu, Cloud-Clone Corp., TX and DTSP10 R and D Systems, MN) according to the manufacturer's instructions.

siRNA transfection

Mouse primary CFs were seeded on plates and cultured to 80% confluence, then transfected with Stat3 siRNA (#sc-29494) or control siRNA (#sc-37007, both Santa Cruz Biotechnology, CA) by using Lipofectamine RNAi MAX transfection reagent (Thermo Fisher Scientific, MA) for 24 hr.

Chromatin immunoprecipitation (ChIP) assay

ChIP was performed as previously reported (*He et al., 2018*) with SimpleChIP Enzymatic Chromatin IP Kits (Cell Signaling Technology, MA) according to the manufacturer's instructions. Briefly, mPCFs were crosslinked with 1% formaldehyde followed by quenching with glycine for 5 min. Cell lysates were digested by micrococcal nuclease, sonicated, and proteins were immunoprecipitated with antibody to STAT3 or rabbit IgG as a control. After complete washing, immunoprecipitated DNA was eluted with elution buffer and reverse-crosslinked overnight at 65°C. DNA was purified and quantified by quantitative RT-PCR. Enrichment was calculated relative to input. Primers for ChIP-qPCR were forward, 5'- TGGCTTCCTCTGTGGTCTCT-3', and reverse, 5'-GTCAAGGTCATGGGATGGTC-3'.

Statistical analysis

Sample sizes were designed with adequate power according to the literature and our previous studies. Data are presented as mean ± standard error of the mean (SEM). Statistical analysis involved use of GraphPad Prism 7 v7.04 with two-tailed, unpaired Student's t test or one-way or two-way ANOVA with Bonferroni multiple comparison post-test, as appropriate. The criterion for statistical significance was $p < 0.05$.

Acknowledgements

Additional information

Author contributions

Qiankun Bao, Resources, Formal analysis, Funding acquisition, Validation, Investigation, Writing - original draft, Writing - review and editing; Bangying Zhang, Kai Zhang, Ming Yuan, Formal analysis, Validation, Investigation; Ya Suo, Formal analysis, Investigation; Chen Liu, Conceptualization, Resources, Investigation; Qian Yang, Resources, Validation, Investigation; Meng Yuan, Resources, Formal analysis, Investigation, Writing - original draft; Yue Zhang, Formal analysis, Funding acquisition,

Writing - original draft; Guangping Li, Conceptualization, Data curation, Supervision, Funding acquisition, Project administration, Writing - review and editing

Author ORCIDs
Qiankun Bao ID https://orcid.org/0000-0002-5221-2780
Chen Liu ID http://orcid.org/0000-0001-7120-5626

Ethics
Human subjects: Ethical approval was obtained through the institutional ethical review board of Peking University People's Hospital (Permit Number: 2018PHB210-01). The study was conducted in accordance with the Declaration of Helsinki. Written informed consent was taken from all study participants.
Animal experimentation: Animal procedures were approved and conducted in accordance with the Experimental Animal Administration Committee of Tianjin Medical University (Permit Number: SYXK 2011-0006; SYXK 2016-0012).

Decision letter and Author response
Decision letter https://doi.org/10.7554/eLife.49923.sa1
Author response https://doi.org/10.7554/eLife.49923.sa2

Additional files

Supplementary files
- Supplementary file 1. RT-PCR primers.
- Transparent reporting form

Data availability
All data generated or analysed during this study are included in the manuscript and supporting files. Source data files have been provided for Figures 1 to 6.

References

Adams JC, Lawler J. 2011. The thrombospondins. *Cold Spring Harbor Perspectives in Biology* **3**:a009712. DOI: https://doi.org/10.1101/cshperspect.a009712, PMID: 21875984

Ali SR, Ranjbarvaziri S, Talkhabi M, Zhao P, Subat A, Hojjat A, Kamran P, Müller AM, Volz KS, Tang Z, Red-Horse K, Ardehali R. 2014. Developmental heterogeneity of cardiac fibroblasts does not predict pathological proliferation and activation. *Circulation Research* **115**:625–635. DOI: https://doi.org/10.1161/CIRCRESAHA.115.303794, PMID: 25037571

Baguet JP, Barone-Rochette G, Tamisier R, Levy P, Pépin JL. 2012. Mechanisms of cardiac dysfunction in obstructive sleep apnea. *Nature Reviews Cardiology* **9**:679–688. DOI: https://doi.org/10.1038/nrcardio.2012.141, PMID: 23007221

Belmadani S, Bernal J, Wei CC, Pallero MA, Dell'italia L, Murphy-Ullrich JE, Berecek KH. 2007. A thrombospondin-1 antagonist of transforming growth factor-beta activation blocks cardiomyopathy in rats with diabetes and elevated angiotensin II. *The American Journal of Pathology* **171**:777–789. DOI: https://doi.org/10.2353/ajpath.2007.070056, PMID: 17640965

Chakraborty D, Šumová B, Mallano T, Chen CW, Distler A, Bergmann C, Ludolph I, Horch RE, Gelse K, Ramming A, Distler O, Schett G, Šenolt L, Distler JHW. 2017. Activation of STAT3 integrates common profibrotic pathways to promote fibroblast activation and tissue fibrosis. *Nature Communications* **8**:1130. DOI: https://doi.org/10.1038/s41467-017-01236-6, PMID: 29066712

Chen L, Einbinder E, Zhang Q, Hasday J, Balke CW, Scharf SM. 2005. Oxidative stress and left ventricular function with chronic intermittent hypoxia in rats. *American Journal of Respiratory and Critical Care Medicine* **172**:915–920. DOI: https://doi.org/10.1164/rccm.200504-560OC, PMID: 15976378

Crawford SE, Stellmach V, Murphy-Ullrich JE, Ribeiro SMF, Lawler J, Hynes RO, Boivin GP, Bouck N. 1998. Thrombospondin-1 is a major activator of TGF-β1 in vivo. *Cell* **93**:1159–1170. DOI: https://doi.org/10.1016/S0092-8674(00)81460-9

Cucoranu I, Clempus R, Dikalova A, Phelan PJ, Ariyan S, Dikalov S, Sorescu D. 2005. NAD(P)H oxidase 4 mediates transforming growth factor-beta1-induced differentiation of cardiac fibroblasts into myofibroblasts.

Circulation Research **97**:900–907. DOI: https://doi.org/10.1161/01.RES.0000187457.24338.3D, PMID: 16179589

Darnell JE, Kerr IM, Stark GR. 1994. Jak-STAT pathways and transcriptional activation in response to IFNs and other extracellular signaling proteins. *Science* **264**:1415–1421. DOI: https://doi.org/10.1126/science.8197455, PMID: 8197455

Gottlieb DJ, Yenokyan G, Newman AB, O'Connor GT, Punjabi NM, Quan SF, Redline S, Resnick HE, Tong EK, Diener-West M, Shahar E. 2010. Prospective study of obstructive sleep apnea and incident coronary heart disease and heart failure: the sleep heart health study. *Circulation* **122**:352–360. DOI: https://doi.org/10.1161/CIRCULATIONAHA.109.901801, PMID: 20625114

Gozal D, Kheirandish-Gozal L. 2008. Cardiovascular morbidity in obstructive sleep apnea: oxidative stress, inflammation, and much more. *American Journal of Respiratory and Critical Care Medicine* **177**:369–375. DOI: https://doi.org/10.1164/rccm.200608-1190PP, PMID: 17975198

He J, Bao Q, Zhang Y, Liu M, Lv H, Liu Y, Yao L, Li B, Zhang C, He S, Zhai G, Zhu Y, Liu X, Zhang K, Wang XJ, Zou MH, Zhu Y, Ai D. 2018. Yes-Associated protein promotes angiogenesis via signal transducer and activator of transcription 3 in endothelial cells. *Circulation Research* **122**:591–605. DOI: https://doi.org/10.1161/CIRCRESAHA.117.311950, PMID: 29298775

Hudon-David F, Bouzeghrane F, Couture P, Thibault G. 2007. Thy-1 expression by cardiac fibroblasts: lack of association with myofibroblast contractile markers. *Journal of Molecular and Cellular Cardiology* **42**:991–1000. DOI: https://doi.org/10.1016/j.yjmcc.2007.02.009, PMID: 17395197

Hugo C, Shankland SJ, Pichler RH, Couser WG, Johnson RJ. 1998. Thrombospondin 1 precedes and predicts the development of tubulointerstitial fibrosis in glomerular disease in the rat. *Kidney International* **53**:302–311. DOI: https://doi.org/10.1046/j.1523-1755.1998.00774.x, PMID: 9461090

Ide M, Ishii H, Mukae H, Iwata A, Sakamoto N, Kadota J, Kohno S. 2008. High serum levels of thrombospondin-1 in patients with idiopathic interstitial pneumonia. *Respiratory Medicine* **102**:1625–1630. DOI: https://doi.org/10.1016/j.rmed.2008.05.009, PMID: 18640828

Ihle JN. 1995. Cytokine receptor signalling. *Nature* **377**:591–594. DOI: https://doi.org/10.1038/377591a0, PMID: 7566171

Jacoby JJ, Kalinowski A, Liu MG, Zhang SS, Gao Q, Chai GX, Ji L, Iwamoto Y, Li E, Schneider M, Russell KS, Fu XY. 2003. Cardiomyocyte-restricted knockout of STAT3 results in higher sensitivity to inflammation, cardiac fibrosis, and heart failure with advanced age. *PNAS* **100**:12929–12934. DOI: https://doi.org/10.1073/pnas.2134694100, PMID: 14566054

Javaheri S, Barbe F, Campos-Rodriguez F, Dempsey JA, Khayat R, Javaheri S, Malhotra A, Martinez-Garcia MA, Mehra R, Pack AI, Polotsky VY, Redline S, Somers VK. 2017. Sleep apnea: types, mechanisms, and clinical cardiovascular consequences. *Journal of the American College of Cardiology* **69**:841–858. DOI: https://doi.org/10.1016/j.jacc.2016.11.069, PMID: 28209226

Kaiser R, Frantz C, Bals R, Wilkens H. 2016. The role of circulating thrombospondin-1 in patients with precapillary pulmonary hypertension. *Respiratory Research* **17**:96. DOI: https://doi.org/10.1186/s12931-016-0412-x, PMID: 27473366

Kasai T, Floras JS, Bradley TD. 2012. Sleep apnea and cardiovascular disease: a bidirectional relationship. *Circulation* **126**:1495–1510. DOI: https://doi.org/10.1161/CIRCULATIONAHA.111.070813, PMID: 22988046

Kumar R, Mickael C, Kassa B, Gebreab L, Robinson JC, Koyanagi DE, Sanders L, Barthel L, Meadows C, Fox D, Irwin D, Li M, McKeon BA, Riddle S, Dale Brown R, Morgan LE, Evans CM, Hernandez-Saavedra D, Bandeira A, Maloney JP, et al. 2017. TGF-β activation by bone marrow-derived thrombospondin-1 causes Schistosoma- and hypoxia-induced pulmonary hypertension. *Nature Communications* **8**:15494. DOI: https://doi.org/10.1038/ncomms15494, PMID: 28555642

Leask A, Abraham DJ. 2004. TGF-beta signaling and the fibrotic response. *The FASEB Journal* **18**:816–827. DOI: https://doi.org/10.1096/fj.03-1273rev, PMID: 15117886

Majack RA, Mildbrandt J, Dixit VM. 1987. Induction of thrombospondin messenger RNA levels occurs as an immediate primary response to platelet-derived growth factor. *The Journal of Biological Chemistry* **262**:8821–8825. PMID: 3597395

Meng XM, Nikolic-Paterson DJ, Lan HY. 2016. TGF-β: the master regulator of fibrosis. *Nature Reviews Nephrology* **12**:325–338. DOI: https://doi.org/10.1038/nrneph.2016.48, PMID: 27108839

Murphy-Ullrich JE, Poczatek M. 2000. Activation of latent TGF-beta by thrombospondin-1: mechanisms and physiology. *Cytokine & Growth Factor Reviews* **11**:59–69. DOI: https://doi.org/10.1016/S1359-6101(99)00029-5, PMID: 10708953

Noman MZ, Buart S, Van Pelt J, Richon C, Hasmim M, Leleu N, Suchorska WM, Jalil A, Lecluse Y, El Hage F, Giuliani M, Pichon C, Azzarone B, Mazure N, Romero P, Mami-Chouaib F, Chouaib S. 2009. The cooperative induction of hypoxia-inducible factor-1 alpha and STAT3 during hypoxia induced an impairment of tumor susceptibility to CTL-mediated cell lysis. *The Journal of Immunology* **182**:3510–3521. DOI: https://doi.org/10.4049/jimmunol.0800854, PMID: 19265129

Patel MK, Lymn JS, Clunn GF, Hughes AD. 1997. Thrombospondin-1 is a potent mitogen and chemoattractant for human vascular smooth muscle cells. *Arteriosclerosis, Thrombosis, and Vascular Biology* **17**:2107–2114. DOI: https://doi.org/10.1161/01.ATV.17.10.2107, PMID: 9351379

Pincha N, Hajam EY, Badarinath K, Batta SPR, Masudi T, Dey R, Andreasen P, Kawakami T, Samuel R, George R, Danda D, Jacob PM, Jamora C. 2018. PAI1 mediates fibroblast-mast cell interactions in skin fibrosis. *Journal of Clinical Investigation* **128**:1807–1819. DOI: https://doi.org/10.1172/JCI99088, PMID: 29584619

Piras BA, Tian Y, Xu Y, Thomas NA, O'Connor DM, French BA. 2016. Systemic injection of AAV9 carrying a periostin promoter targets gene expression to a myofibroblast-like lineage in mouse hearts after reperfused myocardial infarction. *Gene Therapy* **23**:469–478. DOI: https://doi.org/10.1038/gt.2016.20, PMID: 26926804

Ribeiro SM, Poczatek M, Schultz-Cherry S, Villain M, Murphy-Ullrich JE. 1999. The activation sequence of thrombospondin-1 interacts with the latency-associated peptide to regulate activation of latent transforming growth factor-beta. *Journal of Biological Chemistry* **274**:13586–13593. DOI: https://doi.org/10.1074/jbc.274.19.13586, PMID: 10224129

Rogers NM, Sharifi-Sanjani M, Yao M, Ghimire K, Bienes-Martinez R, Mutchler SM, Knupp HE, Baust J, Novelli EM, Ross M, St Croix C, Kutten JC, Czajka CA, Sembrat JC, Rojas M, Labrousse-Arias D, Bachman TN, Vanderpool RR, Zuckerbraun BS, Champion HC, et al. 2017. TSP1-CD47 signaling is upregulated in clinical pulmonary hypertension and contributes to pulmonary arterial vasculopathy and dysfunction. *Cardiovascular Research* **113**:15–29. DOI: https://doi.org/10.1093/cvr/cvw218, PMID: 27742621

Savransky V, Nanayakkara A, Li J, Bevans S, Smith PL, Rodriguez A, Polotsky VY. 2007. Chronic intermittent hypoxia induces atherosclerosis. *American Journal of Respiratory and Critical Care Medicine* **175**:1290–1297. DOI: https://doi.org/10.1164/rccm.200612-1771OC, PMID: 17332479

Schafer S, Viswanathan S, Widjaja AA, Lim WW, Moreno-Moral A, DeLaughter DM, Ng B, Patone G, Chow K, Khin E, Tan J, Chothani SP, Ye L, Rackham OJL, Ko NSJ, Sahib NE, Pua CJ, Zhen NTG, Xie C, Wang M, et al. 2017. IL-11 is a crucial determinant of cardiovascular fibrosis. *Nature* **552**:110–115. DOI: https://doi.org/10.1038/nature24676, PMID: 29160304

Somers VK, White DP, Amin R, Abraham WT, Costa F, Culebras A, Daniels S, Floras JS, Hunt CE, Olson LJ, Pickering TG, Russell R, Woo M, Young T, American Heart Association Council for High Blood Pressure Research Professional Education Committee, Council on Clinical Cardiology, American Heart Association Stroke Council, American Heart Association Council on Cardiovascular Nursing, American College of Cardiology Foundation. 2008. Sleep Apnea and Cardiovascular Disease: An American Heart Association/american College Of Cardiology Foundation Scientific Statement From the American Heart Association Council for High Blood Pressure Research Professional Education Committee, Council on Clinical Cardiology, Stroke Council, and Council On Cardiovascular Nursing. In Collaboration With the National Heart, Lung, and Blood Institute National Center on Sleep Disorders Research (National Institutes of Health). *Circulation* **118**:1080–1111. DOI: https://doi.org/10.1161/CIRCULATIONAHA.107.189375

Su SA, Yang D, Wu Y, Xie Y, Zhu W, Cai Z, Shen J, Fu Z, Wang Y, Jia L, Wang Y, Wang JA, Xiang M. 2017. EphrinB2 regulates cardiac fibrosis through modulating the interaction of Stat3 and TGF-beta/Smad3 signaling. *Circulation Research* **121**:617–627. DOI: https://doi.org/10.1161/CIRCRESAHA.117.311045, PMID: 28743805

Travers JG, Kamal FA, Robbins J, Yutzey KE, Blaxall BC. 2016. Cardiac fibrosis: the fibroblast awakens. *Circulation Research* **118**:1021–1040. DOI: https://doi.org/10.1161/CIRCRESAHA.115.306565, PMID: 26987915

Tyzack GE, Sitnikov S, Barson D, Adams-Carr KL, Lau NK, Kwok JC, Zhao C, Franklin RJ, Karadottir RT, Fawcett JW, Lakatos A. 2014. Astrocyte response to motor neuron injury promotes structural synaptic plasticity via STAT3-regulated TSP-1 expression. *Nature Communications* **5**:4294. DOI: https://doi.org/10.1038/ncomms5294, PMID: 25014177

Unudurthi SD, Nassal D, Greer-Short A, Patel N, Howard T, Xu X, Onal B, Satroplus T, Hong D, Lane C, Dalic A, Koenig SN, Lehnig AC, Baer LA, Musa H, Stanford KI, Smith S, Mohler PJ, Hund TJ. 2018. βIV-Spectrin regulates STAT3 targeting to tune cardiac response to pressure overload. *Journal of Clinical Investigation* **128**:5561–5572. DOI: https://doi.org/10.1172/JCI99245, PMID: 30226828

van Almen GC, Verhesen W, van Leeuwen REW, van de Vrie M, Eurlings C, Schellings MWM, Swinnen M, Cleutjens JPM, van Zandvoort MAMJ, Heymans S, Schroen B. 2011. MicroRNA-18 and microRNA-19 regulate CTGF and TSP-1 expression in age-related heart failure. *Aging Cell* **10**:769–779. DOI: https://doi.org/10.1111/j.1474-9726.2011.00714.x

Wang Z, Li Jia'an, Xiao Wen'ang, Long J, Zhang H. 2018. The STAT3 inhibitor S3I-201 suppresses fibrogenesis and angiogenesis in liver fibrosis. *Laboratory Investigation* **98**:1600–1613. DOI: https://doi.org/10.1038/s41374-018-0127-3

Wei L-H, Kuo M-L, Chen C-A, Chou C-H, Lai K-B, Lee C-N, Hsieh C-Y. 2003. Interleukin-6 promotes cervical tumor growth by VEGF-dependent angiogenesis via a STAT3 pathway. *Oncogene* **22**:1517–1527. DOI: https://doi.org/10.1038/sj.onc.1206226

Wei Q, Bian Y, Yu F, Zhang Q, Zhang G, Li Y, Song S, Ren X, Tong J. 2016. Chronic intermittent hypoxia induces cardiac inflammation and dysfunction in a rat obstructive sleep apnea model. *Journal of Biomedical Research* **30**:490–495. DOI: https://doi.org/10.7555/JBR.30.20160110, PMID: 27924067

Xia Y, Dobaczewski M, Gonzalez-Quesada C, Chen W, Biernacka A, Li N, Lee D-W, Frangogiannis NG. 2011. Endogenous Thrombospondin 1 Protects the Pressure-Overloaded Myocardium by Modulating Fibroblast Phenotype and Matrix Metabolism. *Hypertension* **58**:902–911. DOI: https://doi.org/10.1161/HYPERTENSIONAHA.111.175323

Zhang K, Zhao L, Ma Z, Wang W, Li X, Zhang Y, Yuan M, Liang X, Li G. 2018. Doxycycline Attenuates Atrial Remodeling by Interfering with MicroRNA-21 and Downstream Phosphatase and Tensin Homolog (PTEN)/Phosphoinositide 3-Kinase (PI3K) Signaling Pathway. *Medical Science Monitor* **24**:5580–5587. DOI: https://doi.org/10.12659/MSM.909800